WIND ENERGY
Wind Energ. 0000; **00**:1–16
DOI: 10.1002/we

RESEARCH ARTICLE

Design Optimization of Downwind Land-based Wind Turbines

S. Andrew Ning and Derek Petch

National Renewable Energy Laboratory, Golden, CO, 80401

ABSTRACT

Large wind turbine rotor blades are often constrained by the stiffness required to prevent a tower strike. The mass of these rotor blades may be reducible by utilizing a downwind configuration where the constraints on tower strike are less restrictive. Large upwind and downwind rotors are compared using nonlinear optimization to minimize cost of energy subject to a subset of International Electrotechnical Commission design criteria. The large turbines of this study range in power rating from 5-7 MW and in diameter from 105-175 m. While the focus is on the rotor design, the drivetrain and tower are also optimized. For high-speed wind sites, downwind configurations do not appear advantageous. The decrease in blade mass is offset by increases in tower mass caused by the bending moment from the rotor-nacelle-assembly. For downwind configuration the bending moment of the top mass is additive to that from the thrust loads. For low-wind speed sites the decrease in blade mass is more significant (25-30%) and does show some potential for modest decreases in overall cost of energy (1-2%). Precurving the blades downwind does not appear advantageous. While this does decrease the maximum strain loads, it increases natural frequencies, and decreases annual energy production. Conversely, curving the blades upwind allows for increased power production, and for upwind configurations simultaneously increase tower-strike clearance.

KEYWORDS

downwind rotors, upwind rotors, blade optimization, wind turbine optimization, flexible blades, curved blades

Correspondence
Andrew Ning, NREL, 15013 Denver West Parkway, Golden, CO, 80401.
E-mail: andrew.ning@nrel.gov

Received . . .

NOMENCLATURE

AEP	annual energy production
COE	cost of energy
D	rotor diameter
H	tower height
V_{rated}	rated speed
Ω	rotor rotational speed or frequency
δ	deflection
ϵ	strain
η	safety factor
σ	standard deviation
σ_{VM}	von Mises stress
σ_y	yield stress

Prepared using weauth.cls [Version: 2010/06/17 v1.00]

θ blade twist

c chord

d diameter

f frequency

t thickness

x precurve

1. INTRODUCTION

Reducing the cost of energy of wind turbines requires a careful balance of energy production with capital investment, operational, and maintenance costs. Advances in materials and structural design have enabled taller towers and larger rotors for utility-scale turbines. Larger turbines can produce more power because of the larger swept area of the rotors and the faster wind speeds at higher hub heights. However other design constraints make larger blades increasingly challenging. In the worst-case operating conditions, the blades must be stiff enough to not strike the tower. For upwind cantilevered blades, achieving adequate blade stiffness requires large structural mass, the cost of which may offset any gains in energy production.

One potential avenue to reduce the required blade stiffness is to switch from a traditionally-used upwind configuration to a downwind one. Downwind turbines are less restricted by tower-strike, and from a stiffness standpoint are constrained primarily by frequency response and buckling constraints. Increased fatigue damage from the tower shadow becomes a concern, but may be alleviated through aerodynamic fairing on the tower or other means [1]. A recent study by Resio on downwind turbines suggested that blade mass could be reduced by 20% with a corresponding 5% reduction in blade fatigue loads without sacrificing power [2]. This study found that benefits to the blades came at the expense of a 20% larger tower bottom bending moment, although no assessment was made on the corresponding impact to the tower mass or system costs. They also showed that while even more flexible blades were feasible, they led to decreases in power production. Other system benefits of downwind turbines have been suggested in the literature. A wind plant study by Yoshida suggested that downwind turbines would be beneficial in complex terrains because the terrain topology often induces an upward flow and the tilt of downwind turbines is much closer to perpendicular to the incoming wind [3]. Reiso and Moe [4] discuss how downwind turbines enable simpler yaw systems, which can lead to significant maintenance cost reductions, especially offshore.

An additional concept, highlighted in a recent study, suggests that significantly increasing the blade curvature for downwind turbines may yield additional benefits [5]. Precurved blades would reduce bending moments along the blade and subsequently the strain. This conceptual study suggested that significant mass reductions would be possible with precurved blades. However, the study used only one constraint in resizing the rotor blades (stress distribution at rated speed), and did not include other important sizing constraints such as natural frequencies, panel buckling, and strain in survival loads. Furthermore the design was optimized for minimum mass, while ignoring power production or other factors affecting cost of energy.

This study is concerned with comparing large land-based upwind and downwind rotors using the same design criteria to estimate the potential system benefits of downwind configurations. Additionally, we investigate the impact of blade precurvature in the context of cost of energy trade-offs. Nonlinear optimization and design criteria, primarily that of the International Electrotechnical Commission (IEC) [6], are used to size the turbines.

2. METHODOLOGY

The design methodology extends that described previously by Ning [7], but with much more detailed tower modeling, a new drivetrain model, a larger number of design variables, and improved and expanded constraint handling. Many of these additions are described in a recent study on high tip-speed rotors [8]; additional improvements in the rotor modeling for curved or highly flexible blades are discussed below. Table I summarizes the methodology used for the physics-based portions of the analysis; additional detail is provided by Ning [7, 8] and in the following subsections. The methodology for the physics-based hub and drivetrain models are discussed in a separate publication [9]. Turbine capital costs were estimated using recently developed mass-based cost models [10]. Balance-of-station costs used a recently developed bottom-up model for land-based turbines [11]. Operations and maintenance costs came from the NREL cost and scaling model [12].

Wind Energ. 0000; **00**:1–16 © 0000 John Wiley & Sons, Ltd.
DOI: 10.1002/we
Prepared using weauth.cls

Discipline	Theories	Codes
Blade aerodynamics	Blade element momentum	RotorSE, CCBlade
Blade structures	Beam finite element, classical laminate theory	RotorSE, pBEAM CurveFEM, PreComp
Tower aerodynamics	Power-law wind profile, cylinder drag	TowerSE
Tower structures	Beam finite element, Eurocode, Germanischer Lloyd	TowerSE, pBEAM
Nacelle sizing and structures	University of Sunderland and WindPACT	DriveSE

Table I. Wind turbine analysis methods.

The rotor and tower models are physics-based models with dimensions sized using nonlinear optimization. The nacelle uses physics-based models for some components, and sizing tools for other components using a model from the University of Sunderland [13], with dimensions scaled from WindPACT studies [14]. Even though the focus of the study was on rotor design, including the nacelle and tower in the optimization process was important because of the range of rotor diameters and power ratings explored.

Although the blade geometry and thickness of the laminate stacks were optimized, the laminate schedules were kept constant. Laminate schedule optimization involves a large number of discrete variables, and the additional complexity was unwarranted for the purposes of this study. The laminate schedule used in this study came from Sandia National Laboratory and was designed to approximately match the structural distributions specified by the NREL 5-MW reference model, while simultaneously satisfying IEC load requirements [15]. The total thickness of the spar-cap and aft-panel laminates were sized directly by the optimization, while leading-edge panels and shear webs were indirectly sized relative to the section thickness. Airfoil profiles (for unit chord) are also fixed to not introduce additional complexity and uncertainty in trying to estimate aerodynamic performance of very thick sections.

2.1. Rotor Analysis

The rotor analysis was based on steady aeroelastic loading primarily using blade element momentum theory, classical laminate theory, and beam finite element theory. The study by Resor [15] was used to validate and in some cases calibrate the various design constraints for the baseline NREL 5-MW design. The aerodynamic performance and structural design constraints for the rotor are discussed in the following subsections. Downwind rotors that may utilize highly flexible blades required some unique considerations as highlighted below.

2.1.1. Power Production

Flexible blades can undergo significant deflection under load. This out-of-plane blade bending involves a coupling between the aerodynamic loading and the structural deformation. If the downwind deflection of the blade is not considered when generating power curves, than the AEP is generally significantly overpredicted. The coupled aero/structural solution of the deflected blade shape was found using an internal fixed point iterator between the blade aerodynamics and structural analyses converged to a tolerance of 1×10^{-8}, repeated at every analysis iteration. For purposes of computing AEP, recomputing the blade deflection at every point along the power curve would have significantly increased computational time. Power curves were generated for a number of configurations with the aerodynamics and structures fully coupled throughout the power curve, and the annual energy production was found to agree well by using the deflection for a wind speed around 70% of the rated speed. For all AEP calculations, the out-of-plane structural deformation of the blade at 70% of the rated speed was used throughout the power curve. Including the downwind structural deflection in the power calculation had only a small impact on upwind designs because of the high stiffness. However, for downwind designs that have the potential for significantly decreased blade stiffness, capturing this trade-off in power production loss was very important.

2.1.2. Tower and Ground Strike

The maximum out-of-plane tip deflection was constrained to avoid tower strike for upwind configurations. The study by Resor [15] found that the maximum out-of-plane deflection for this blade occurred at IEC DLC 1.3 extreme turbulence

model (ETM).* The out-of-plane blade tip deflection is maximum near rated speed. Tip deflection was estimated at 180° azimuth with the nominal wind speed at V_{rated} with a 3σ gust. The standard deviation for the turbulence was estimated from the ETM for a "category B" level of turbulence. Because the deflection is computed under static loading, a calibration factor for dynamics was added. Both the studies by Jonkman [16] and Resor [15] used NREL's aeroelastics code FAST and estimated the maximum out-of-plane tip deflection for this blade to be around 5.6 m. The tip deflection computed from the static analysis was multiplied by 1.35 to correct for the dynamic effects and better match these results. Both the computation of the total loads (aerodynamic + inertial + centrifugal) and the transformation of the tip deflection into the tower coordinate system needed to account for the curvature of the blade.

The allowable deflection was a function of the blade length, curvature, precone and tilt angles, and the tower dimensions. The available clearance was reduced using a total safety factor of $\eta_{dfl} = 1.485$ (1.35 loads, 1.1 materials, and 1.0 consequences of failure). The resultant constraint was imposed as:

$$\delta_{tip}\ \eta_{dfl} \leq \delta_{max} \tag{1}$$

Similarly, the clearance between the ground and the blade tip was computed and constrained to be at least 20 m. Local ordinances have significant variability in minimum ground clearance requirements, but for this study it was never an active constraint anyway.

$$\delta_{ground} \geq 20 \tag{2}$$

2.1.3. Natural Frequencies

In order to estimate natural frequencies for curved blades, the existing code CurveFEM [17] was incorporated into the analysis. CurveFEM was designed to compute natural frequencies for blades with precurve and presweep. The estimated natural frequencies for the baseline design agree well with those from the previous published studies on the NREL 5-MW reference model [15, 16]. The first flapwise mode (and consequentally all modes) was constrained to be 10% larger than the maximum blade passing frequency.

$$f_0 \geq 1.1\ n_{blades}\Omega_{rated} \tag{3}$$

2.1.4. Ultimate Strength

Axial strain was computed under a combined loading condition with a 50-year survival wind at 90° to the pitch axis and the blade in the 12 o'clock position (approximately the worst-case loading condition for this blade). Strain was computed at the outer edge of the airfoil in the midpoint of the panel for both the spar-cap panels and the trailing-edge panels. The strain at each section was multiplied by the safety factor $\eta_{str} = 1.755$ (1.35 loads, 1.3 materials, and 1.0 consequence of failure). For the spar cap it was assumed that the ultimate strain was 10,000 microstrain in both tension and compression, which is a representative conservative value for the materials used in the blade. For the trailing-edge panels the maximum strain was assumed to be 2,500 microstrain per GL guidelines [18]. The Sandia study also found IEC DLC 6.1 extreme wind speed model to be the critical ultimate strain condition. While they did not do a combined load case, the magnitudes show reasonable agreement.

The constraint is only applied at a subset of the stations. Because the strain varies smoothly, this allows the number of constraints to be reduced without affecting the solution (an assumption which is always checked for any optimized solutions). The constraint is applied as

$$-\epsilon_{ult} \leq \epsilon\ \eta_{str} \leq \epsilon_{ult} \tag{4}$$

2.1.5. Panel Buckling

The constitutive equations for a laminate sequence can be expressed as

$$\left[\begin{array}{c} N \\ \hline M \end{array}\right] = \left[\begin{array}{c|c} A & B \\ \hline B & D \end{array}\right] \left[\begin{array}{c} \epsilon^0 \\ \hline k \end{array}\right] \tag{5}$$

*The study actually showed DLC 1.4 extreme direction change (EDC) as the condition producing the largest deflection, however only a PI controller was used for speed regulation and no controller logic was asserted for start-up and shutdowns. The controller response to ECD, had there been one, would have substantially reduced turbine loads and resulted in turbine shutdown in the event of an extreme direction change.

Wind Energ. 0000; **00**:1–16 © 0000 John Wiley & Sons, Ltd.
DOI: 10.1002/we
Prepared using weauth.cls

where N and M are the average forces and moments of the laminate per unit length, and ϵ^0 and k are the mid-plane strains and curvature (see Halpin). [19]. The D matrix is a 3×3 matrix of the form[†]

$$\begin{bmatrix} D_{11} & D_{12} & 0 \\ D_{12} & D_{22} & 0 \\ 0 & 0 & D_{66} \end{bmatrix} \tag{6}$$

The critical buckling load for long (length greater than twice the width) simply supported panels at a given section is estimated as [20]:

$$N_{cr} = 2\left(\frac{\pi}{w}\right)^2 \left[\sqrt{D_{11}D_{22}} + D_{12} + 2D_{66}\right] \tag{7}$$

where w is the panel width. The critical strain is then

$$\epsilon_b = -\frac{N_{cr}}{T\,E} \tag{8}$$

where T is the total thickness of the laminate stack, E is the effective axial modulus of elasticity for the stack, and the negative sign accounts for the fact that the strain is compressive in buckling.

Buckling was checked on the spar cap and aft panels. ANSYS simulations suggest that the baseline 5-MW design is very close to the buckling margin after applying the safety factors [15]. The distribution of the critical buckling load agreed reasonably well with those of the Sandia report when the safety factor were not applied to these results.

Like the ultimate strain calculation the constraint need only be applied a subset of the radial stations. The constraint is given as:

$$\epsilon \leq \epsilon_b \tag{9}$$

2.1.6. Additional Rotor Constraints

For all designs, the rotor tip speed was constrained to be less than 80 m/s. This constraint was applied directly in the analysis. The maximum chord was constrained to be less than 5.3 m for consistency with road-based transportation constraints. The root bolt circle diameter was assumed to be 2.5% of the rotor diameter.

2.2. Tower Analysis

The towers optimized in this study were assumed to be steel tubular designs. Tower structural analysis was based on beam finite element analysis with 20 beam elements along the tower. It was assumed that the driving load cases for structural strain were the operational condition IEC DLC 1.3 with the extreme turbulence model (ETM), and the parked survival case IEC DLC 6.2. The ETM condition was approximated by computing rotor and tower loading at $V_{rated} + 3\sigma$ where the standard deviation for the ETM came from a class B site. For the survival case, it was assumed that one of the blades experienced a pitch failure and was thus unfeathered. The predicted static thrust from the rotor was multiplied by a dynamic amplification factor of 1.8 to give better agreement with published FAST simulations [21]. Wind loading on the tower was estimated using a simple power-law profile, with drag coefficients for two-dimensional flow around a cylinder. Hoop stress was estimated using the methodology described by Eurocode [22]. The axial, shear, and hoop stress along the downwind side of the tower were combined into an equivalent von Mises stress. This stress was multiplied by a total safety factor of 1.485, and constrained to be less than the yield stress of 345 MPa. Like the rotor, the stress constraint was applied at a few subsections for efficiency.

Shell buckling was estimated using the methodology described by Eurocode [22] for a tapered cylinder with a safety factor of 1.35 for the loads, and 1.1 for buckling resistance. It was assumed the tower was reinforced every 30 m along the tower to decrease the effective buckling length. Global buckling was estimated using the methodology from Germanischer Lloyd [23] with the same safety factors.

Tower frequencies were constrained to be 10% higher than the rotor rotation frequency at rated conditions. In computing the frequency response of the tower, the rotor-nacelle assembly was treated as a rigid object offset from the tower top with mass properties supplied by the rotor and nacelle analyses.

A minimum tower diameter of 3.87 m was set to facilitate the connection of the nacelle and yaw-bearing. A maximum tower diameter of of 6.3 was set to facilitate road-based transportation[‡]. To promote weldability of the tower sections, the diameter to thickness ratio was constrained to be greater than 120. For manufacturability the tower top diameter could not

[†] Not all laminates in the blade are balanced and symmetric and so the zero entries in the matrix are actually nonzero. However, the magnitude of these terms is very small for the laminates studied here and are thus well approximated as specially orthotropic.

[‡] While it is difficult to set a precise number on the upper bound of what is transportable, land-based tubular towers of this size have recently been developed [24]

be smaller than 40% of the tower base diameter. The tower constraints are summarized as:

$$\begin{aligned} f_0 &\geq 1.1\,\Omega_{max} \\ \eta_t\,\sigma_{VM1.3} &\leq \sigma_y \\ \eta_t\,\sigma_{VM6.2} &\leq \sigma_y \\ shell\ buckling_{1.3} &\leq 1 \\ shell\ buckling_{6.2} &\leq 1 \\ global\ buckling_{1.3} &\leq 1 \\ global\ buckling_{6.2} &\leq 1 \\ d_{top} &\geq 0.4\,d_{base} \\ d/t &\geq 120 \end{aligned} \tag{10}$$

2.3. Nacelle

A new drivetrain model was developed as detailed by its authors in a separate publication [9]. Some drivetrain components were modeled with scaling relationships (bearings, yaw system, generator), while others used bottom-up physics models (bedplate, gearbox, low-speed shaft). For the purposes of facilitating gradient-based optimization in this study, each of the models was modified slightly in order to produce output that was continuously differentiable. This including fitting splines to look-up tables for bearing masses, moving internal sizing routines to constraints at the system-level optimization, and replacing any nondifferentiable function (e.g., min, max, abs) with differentiable versions.

The bedplate was modeled with two I-beams. For simplicity the nondimensional proportions of each I-beam were kept constant, and the total height of each was used a design variable. The forward and aft I-beams were sized independently, each with constraints on bending stress and deflection. The low-speed shaft used a distortional energy failure theory. The design variables included the total shaft length, and the distance between bearings. Maximum deflections were applied as constraints. The gearbox had its own internal optimization, modifying the stage speed ratios to minimize its weight. The results of this optimization were smooth and simple enough to be kept internal to the system-level optimization. The constraints for the drivetrain are summarized as:

$$\begin{aligned} \sigma_{bedplate-fore} &\leq \sigma_{max} \\ \sigma_{bedplate-aft} &\leq \sigma_{max} \\ \delta_{bedplate-fore} &\leq \delta_{max} \\ \delta_{bedplate-aft} &\leq \delta_{max} \\ -\delta_{max} \geq \delta_{lss} &\leq \delta_{max} \end{aligned} \tag{11}$$

2.4. Optimization

To reduce the number of design variables, distributed variables of interest were specified at a number of discrete locations along the blade and an Akima spline was used to define the variable in a continuous manner along the blade. All variables were defined on a normalized blade and subsequently made dimensional using the rotor hub and tip radii. Blade chord was specified at four points, with the location of max chord as an additional variable (Figure 1a). Twist was defined at four radial stations with a constant value across the cylindrical sections (Figure 1b). The spar cap thickness distribution used a multiplier across the cylinder section, and a spline across the outer portion of the blade with four control points (Figure 1c). For the aft panels, the reference model uses a step-like distribution of thickness, and that type of parameterization was preserved. A multiplier was used across the cylinder section, and the thickness was defined as a constant value across four sections along the outer portion of the blade (Figure 1d). In this analysis, precurve was defined as the offset distance of the blade normal to the nominal blade reference axis (positive downwind). For cases with precurve, the precone angle was fixed at zero, otherwise the rotor diameter would be coupled to precurve. The reference blade has no precurve, but Figure 1e shows an example of the parameterization for a curved blade.

The nacelle variables included the bedplate I-beam height (fore and aft), and the lengths in the low-speed shaft, as discussed previously. The tower was parameterized as two linear tapered sections as shown in Figure 2. The waist location was normalized by the tower height. A summary of all the design variables is provided in Table II.

Optimizations were performed using SNOPT [25], a package for nonlinear optimization problems using the sequential programming method, and were formulated in the OpenMDAO framework [26]. All constraints were scaled to be of order one for improved optimization convergence. Analytic gradients were derived for all of the aerodynamic modules, cost modules, finance modules, and for some of the structural modules. Modules were broken up in to many smaller submodules to facilitate ease in deriving gradients. Some of these gradients were derived by hand, while others were computed using automatic differentiation (Tapenade [27] and AlgoPy). An adjoint method was used to compute total derivatives for the

Wind Energ. 0000; **00**:1–16 © 0000 John Wiley & Sons, Ltd.
DOI: 10.1002/we
Prepared using weauth.cls

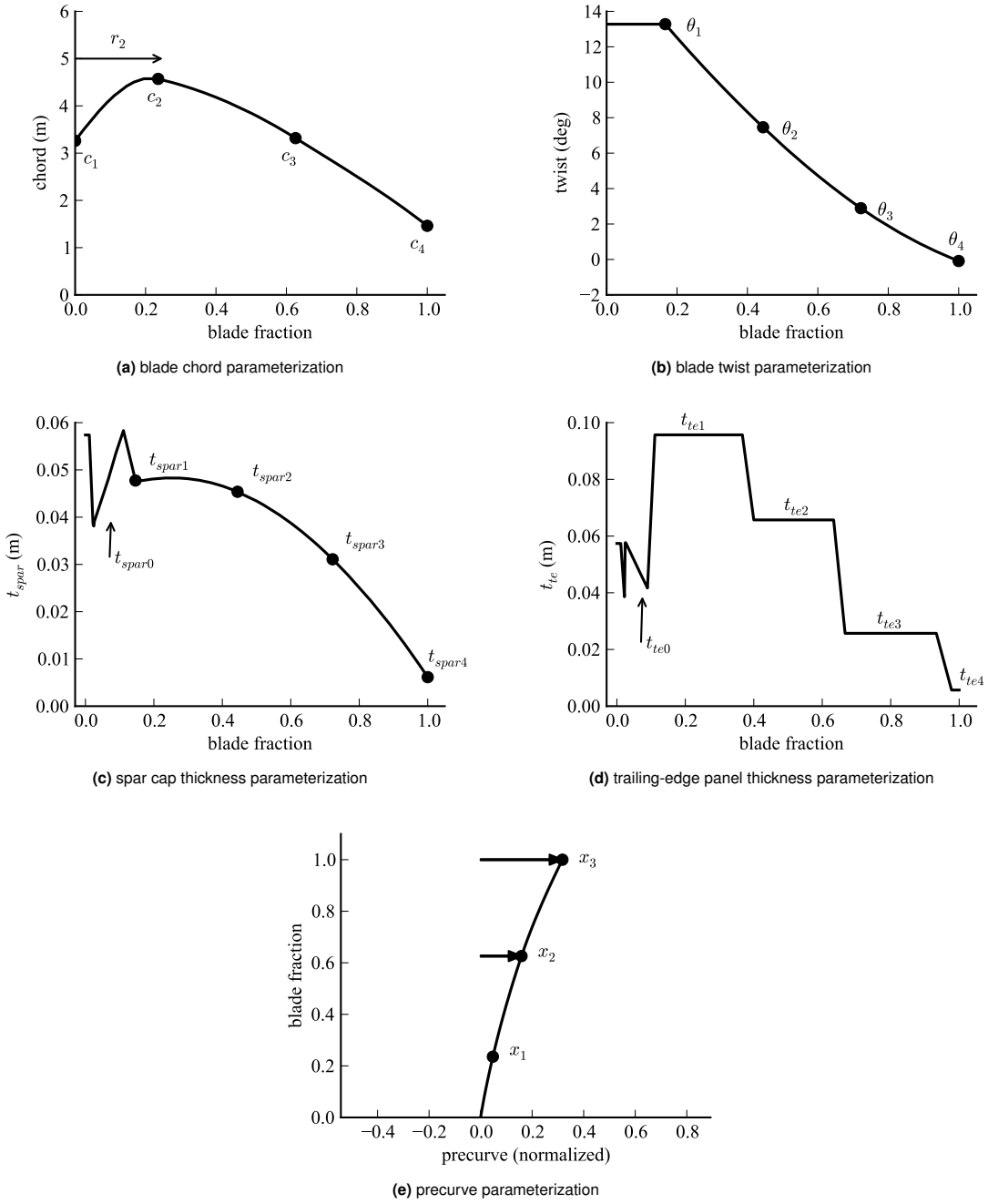

(a) blade chord parameterization

(b) blade twist parameterization

(c) spar cap thickness parameterization

(d) trailing-edge panel thickness parameterization

(e) precurve parameterization

Figure 1. Parameterization of some of the design variables used in defining the rotor blade geometry.

rotor aerodynamics analysis (CCBlade). Missing derivatives related to the structural analysis were estimated using finite differencing. Total system derivatives were computed using the unified chain rule approach described by Martins and Hwang [28] as implemented in OpenMDAO . Because there were a larger number of constraints as compared to design variables, a forward method was used. OpenMDAO also computed the coupled aero/structural derivatives around the fixed point iteration used to solve blade deflection, and the coupled derivatives around the Brent solver used in the power curve module to find rated speed. The benefits of using analytic derivatives, as opposed to finite differencing, for this problem are highlighted in a recent publication [29].

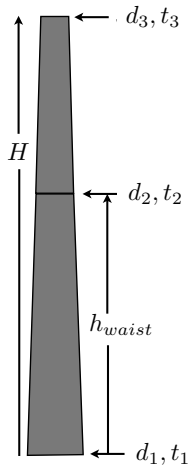

Figure 2. Tower parameterization.

Table II. Design variables used in optimization.

description	symbol	parameters
blade chord distribution	c	5
blade twist distribution	θ	4
spar cap thickness distribution	t_{spar}	5
aft panel thickness distribution	t_{aft}	5
blade precurve distribution	$x_{precurve}$	3
target tip-speed ratio in Region 2	λ_2	1
low-speed-shaft lengths	L_{shaft}	2
bedplate I-beam sizing	h_{beam}	2
tower height	H	1
tower waist location	h_{waist}	1
tower diameter	d	3
tower wall thickness	t_{wall}	3

3. DOWNWIND ROTORS

This section explores the performance of downwind rotors as compared to upwind rotors for three cases: 5-MW machines in Class I wind sites, 5-MW machines in Class III wind sites, and 7-MW machines in Class III wind sites. All designs used a precone angle of 2.5 degrees, a tilt angle of 5 degrees, and no precurve. For both upwind and downwind machines, the direction for tilt and precone was such that the separation distance between the blades and the tower increased. All designs were optimized for minimum cost of energy with the same set of constraints, except that the tower-strike deflection constraint was removed for downwind configurations.

Figure 3 compares the cost of energy, annual energy production, blade mass, and tower mass as a function of rotor diameter for 5-MW machines in a Class I wind site. Each point in the curves represents an optimized design for a given diameter. For these design conditions, switching to a downwind design does not seem to provide any benefit. The downwind configurations does allow for significant savings in blade mass of 12% at 125 m diameter (Figure 3c). At the high wind speeds of Class I sites, the survival wind speed is a driving design condition and affects both the upwind and downwind designs in essentially the same way. Thus, alleviating the tower strike constraint does not provide as significant of an advantage as one might expect. Additionally, the cost savings from lighter blades is offset by a cost increase from a heavier tower (Figure 3d). For an upwind design, the weight of the rotor-nacelle-assembly (RNA) provides a bending moment along the tower in the opposite direction to that caused by the rotor thrust. In contrast, for downwind configurations, the bending moment from the RNA weight is additive, meaning that a heavier tower is required.

The downwind designs have slightly lower annual energy production because the operational loads deflect the blades away from a vertical position where energy production is maximized (the opposite occurs for the upwind designs to a limited extent depending on the tilt and precone angles), but the impact is slight (Figure 3b. The minimum cost of energy for downwind configurations is slightly higher than the minimum cost of the upwind configurations. For these design conditions, downwind configurations do not appear to be advantageous.

The study was repeated for 5-MW designs in a Class III wind site. Large scale development potential exists for turbines optimized for low wind speed applications. Figure 4 shows the changes in cost of energy, annual energy production, blade mass, and tower mass as a function of rotor diameter. For this lower wind speed class, the downwind configurations do show an advantage. The reduction in blade mass is more significant. At a diameter of 145 m, the downwind configurations utilize blades that are 30% lighter than the corresponding upwind design. Because the power rating is the same as the previous set of results, the maximum tip deflection in operational conditions is similar. However, for this lower wind speed site, the survival wind speeds are lower and the tower strike constraint becomes a much more dominant constraint. Thus, the benefit to switching to a downwind configuration is more pronounced.

Like, the previous case, the disadvantages of the downwind configuration lead to heavier towers (18% heavier), and lower AEP (1% lower). Still, the minimum cost of energy downwind design has a 1.5% lower cost of energy than the minimum cost of energy upwind design. The optimal downwind design occurs at a larger diameter than does the optimum upwind design.

Wind Energ. 0000; **00**:1–16 © 0000 John Wiley & Sons, Ltd.
DOI: 10.1002/we
Prepared using weauth.cls

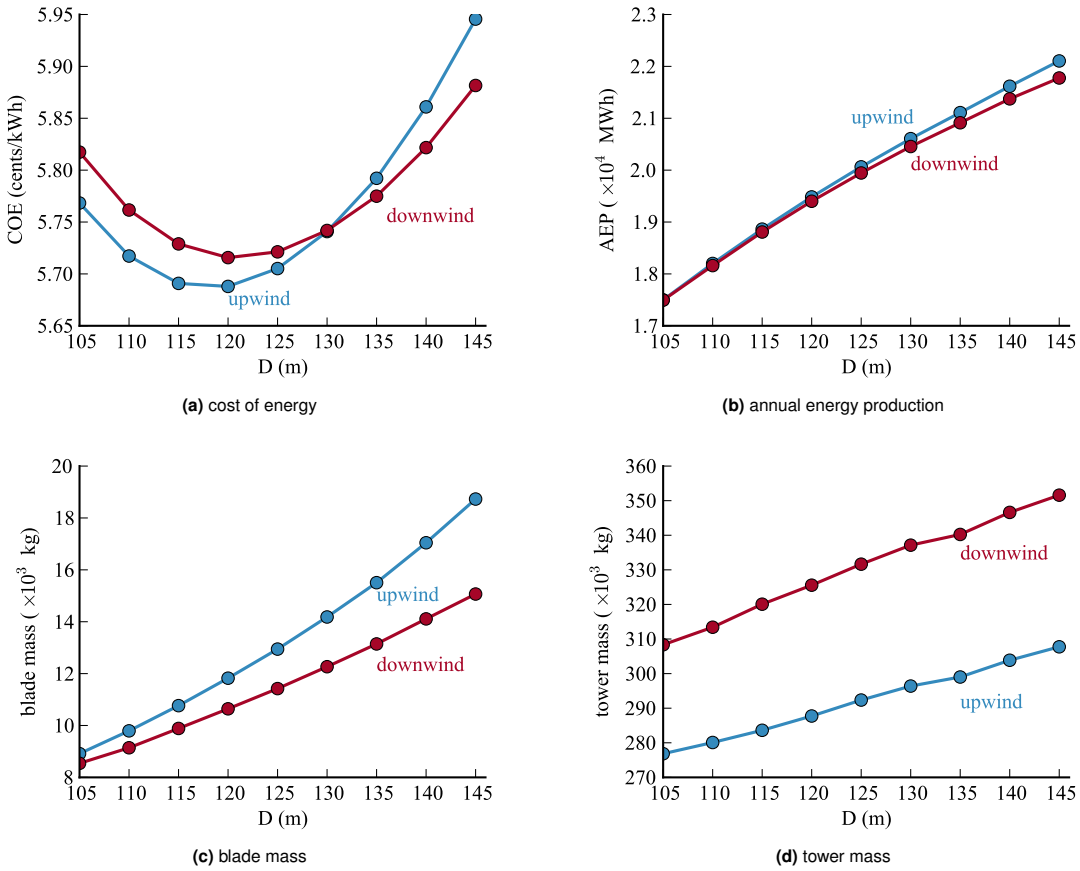

(a) cost of energy

(b) annual energy production

(c) blade mass

(d) tower mass

Figure 3. Variation in performance with rotor diameter for upwind and a downwind configurations (Class I wind, 5.0-MW rating).

The last case explores larger 7-MW designs. Figure 5 shows the changes in cost of energy, annual energy production, blade mass, and tower mass as a function of rotor diameter. The benefits are similar to the 5-MW Class III case. For a given wind class, one would expect that turbines with higher power ratings would benefit to a larger degree from a downwind configuration. A larger machine rating translates into larger maximum tip deflections, increasing the potential benefit of alleviating the tower-strike constraint. However, the design approach could certainly be improved for these larger machines. While the total thickness of the laminate stacks was optimized, the same layup sequence and nondimensional airfoil profile that was designed for the 5-MW reference model was used. Furthermore, only tubular steels towers were explored within the scope of this study. More efficient turbines are likely to be found by utilizing hybrid or truss-style towers, and incorporating additional carbon in the blades. Regardless, significant savings in blade mass are apparent from switching to a downwind configuration for these Class III wind sites. Whether or not that translates into significant system cost savings depends on detailed design decisions of downwind configurations and how that impacts tower mass, performance losses from blade flexibility, and performance losses and increased fatigue damage from operating in a tower shadow.

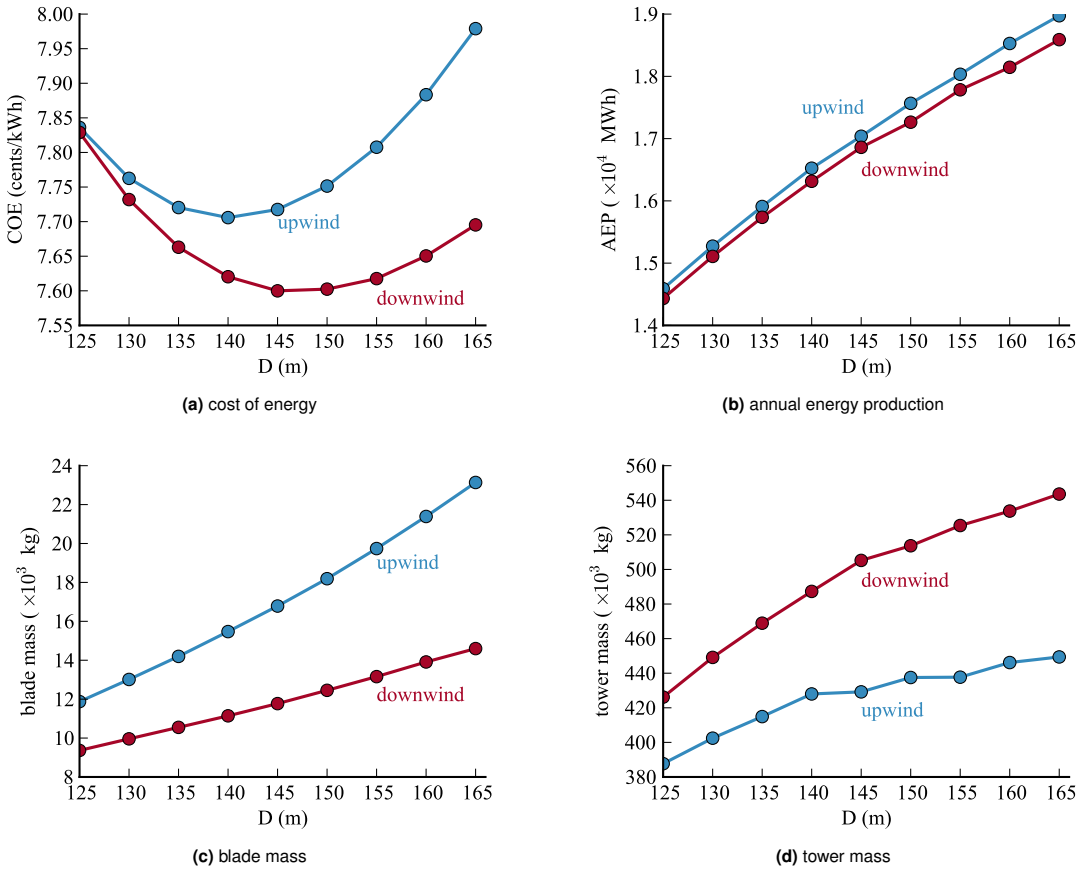

(a) cost of energy

(b) annual energy production

(c) blade mass

(d) tower mass

Figure 4. Variation in performance with rotor diameter for upwind and a downwind configurations (Class III wind, 5.0-MW rating).

Wind Energ. 0000; **00**:1–16 © 0000 John Wiley & Sons, Ltd.
DOI: 10.1002/we
Prepared using weauth.cls

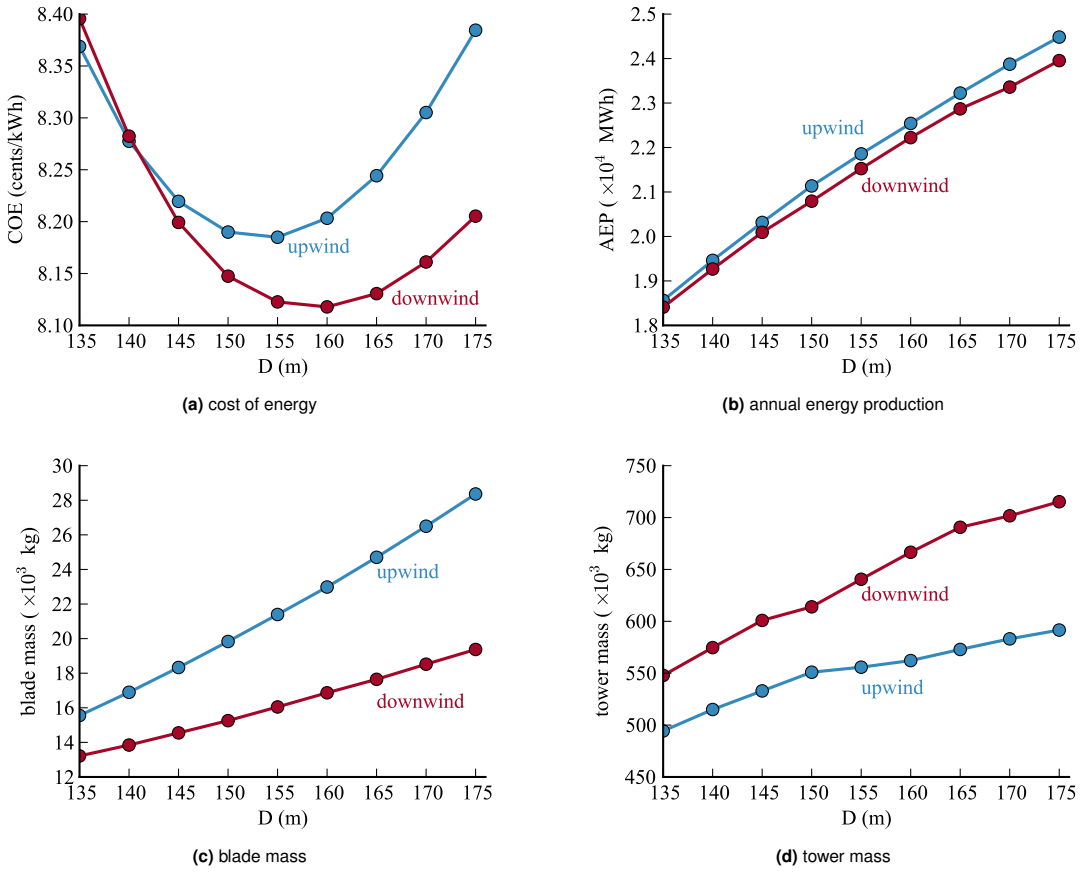

(a) cost of energy

(b) annual energy production

(c) blade mass

(d) tower mass

Figure 5. Variation in performance with rotor diameter for upwind and a downwind configurations (Class IIII wind, 7-MW rating).

4. PRECURVED DOWNWIND BLADES

Conceptual studies suggest that very large mass reductions are possible by precurving the blade downwind for downwind rotors [5]. By aligning the blades in the direction of the local combined loading (aerodynamic, weight, centrifugal), the bending loads are significantly reduced and thus a lighter structure is possible. An analysis was done comparing a straight blade with 0 degrees precone, with a blade with the precurve angle aligned with the load direction (an average of the aligned precurve for 0° and 180° azimuth). Both blades have the same diameter, which implies that the precurved blade is longer. No additional sizing was performed for this comparison. The reference axis for both blades can be seen in Figure 6. Table III summarizes some of the major changes in the design criteria. The data shows that indeed the strain at the operational condition is decreased dramatically (37% reduction), however the survival loading condition is generally the more critical case for blade sizing. Because there are no centrifugal loads at the survival loading condition, or at least greatly diminished centrifugal loads, the local force angle is tilted downwind and the benefits of precurvature are far less dramatic (only a 4% reduction in max strain). Furthermore, the curvature of the blades creates a longer blade, which results in significantly lower natural frequencies. Resonance avoidance of the blades is often a driving constraint which would further reduce the advantage of the longer blade. Even ignoring the other structural constraints, we see that this design results in about a 4% loss in annual energy production. Even if the reduced loading were to allow for a lighter more flexible structure, the energy production would drop even more than it would for a stiff blade. Although the precurved blades do have the same swept area, the significant curvature toward the tips results in reduced incoming velocity normal to the blades with a corresponding loss in power production.

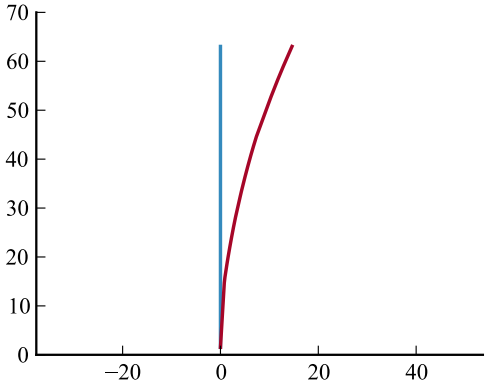

Figure 6. Profile of downwind blade with fixed precone and highly curved blade based on minimizing bending-loads at rated conditions.

	straight blade	curved blade
max strain at rated (microstrain)	1,336	841
max strain at survival (microstrain)	3,001	2,872
1st flap frequency (Hz)	0.961	0.848
1st edge frequency (Hz)	1.15	1.08
AEP (MWh)	19,560	18,802

Table III. Comparison of straight blade and curved blade concept.

Downwind rotors with blades curved downwind generally suffer from significant power loss. The very features that makes them advantageous structurally, namely decreased loading and high flexibility, are disadvantageous aerodynamically. The decreased loads, particularly near the tip, generally correspond to decreased power, and the high flexibility causes additional deflection and shedding of load with even more power loss. To demonstrate the magnitude of the effect, two parameter sweeps are examined, both for the NREL 5-MW reference model operating downwind. In the first, the blade precone angle is varied from 0 to 30 degrees for a downwind turbine. In the second sweep the blade curvature is increased such that curvature varies smoothly and the maximum tip deflection covers the same range as the

Wind Energ. 0000; **00**:1–16 © 0000 John Wiley & Sons, Ltd.
DOI: 10.1002/we
Prepared using weauth.cls

precone sweep. The corresponding precone angle that produces the same precurved tip deflection is called the "effective precone angle". In all cases, the swept area of the rotor is kept constant and so the blade length is elongated as needed. The blade profile for 0, 10, 20, and 30 degrees (effective) precone is shown for both sweeps in Figure 7. The corresponding variation in power coefficient (and thus in power because the swept area is constant) is shown in Figure 8. For flexible blades, the precurve sweep is the more relevant one because the structural deflection leads to curved shapes more like those seen in Figure 7b.

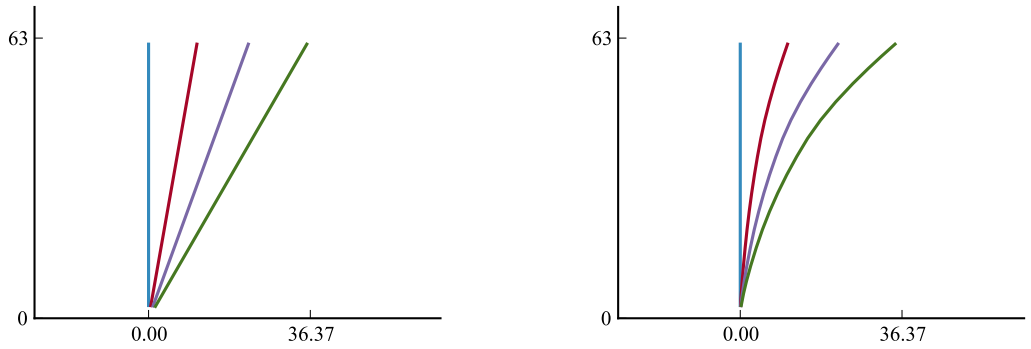

(a) Blade profile for 0, 10, 20, and 30 degrees precone.

(b) Blade profile for 0, 10, 20, and 30 degrees effective precone (same tip deflection but using a curved shape).

Figure 7. Blade profiles for preconed and precurved blades.

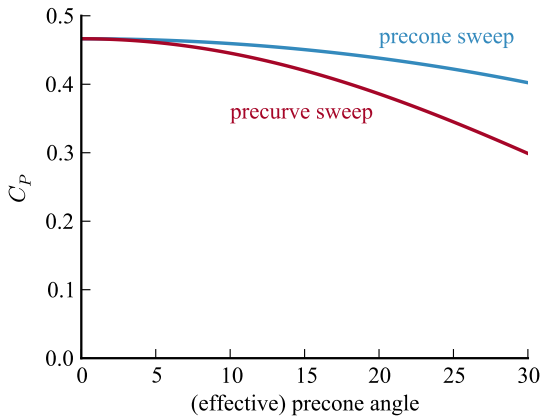

Figure 8. Power loss with increased precone or precurvature. For blades with curvature, as occurs due to structural deformation, the loss of power is particularly pronounced.

The loss of power is caused primarily by the decrease in the magnitude of the velocity normal to the blade profile, especially at the blade tips. While the blades do increase in length in order to maintain capture area, the reduced normal velocity component is a larger effect. As the blades curve away from vertical, a greater fraction of the incoming velocity is redirected radially along the blade. Three-dimensional effects caused by spanwise flow are not captured by BEM theory, but it is not expected that those effects would lead to significant beneficial power increases. Figure 9 shows the torque per unit length along the blade length for the coned and curved blades shown in Figure 7 at 0 degrees azimuth. The total instantaneous power is proportional to the integral of the curves. We see that the blade lengths do get longer leading to greater power capture, but that increase is more than offset by the decrease in peak torque loads leading to lower overall power production. Downwind precurvature could be highly beneficial if the structural response of the blades could be tailored to be stiff and oriented in a nearly vertical orientation around rated speed, but would respond flexibly and shed loads near survival wind conditions.

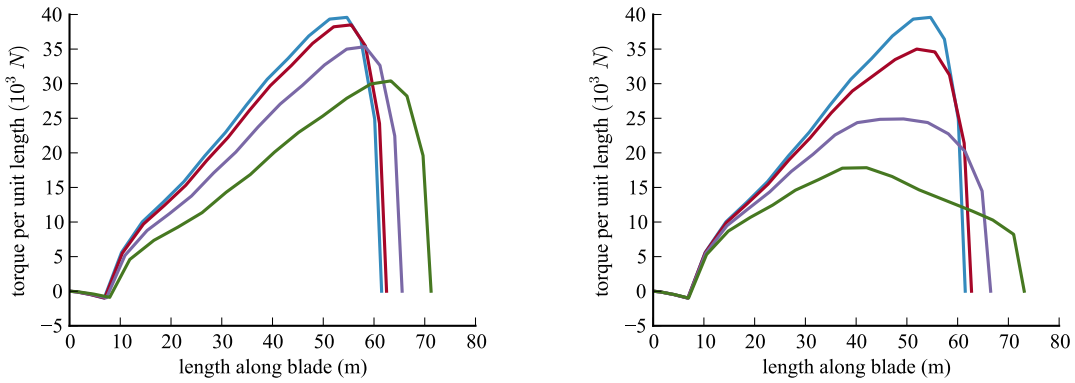

(a) Torque per unit length along blades precurved at 0, 10, 20, and 30 degrees.

(b) Torque per unit length along blades curved with an effective precone angle of 0, 10, 20, and 30 degrees.

Figure 9. Variation in torque per unit length along coned and curved blades. The instantaneous power production is proportional to the area under the curves. Each curve corresponds to a profile shown in Figure 7

A final case was examined where the optimizer was allowed to optimize the precurvature. A downwind 5-MW turbine at a Class III site was optimized for minimum cost of energy. The diameter was set at 145 m, which was approximately the optimal diameter for this configuration (Figure 4a). The optimized shape of the blade both unloaded, and at $0.7\,V_{rated}$ is shown in Figure 10. The blade is actually precurved upwind, in the opposite direction of the blades discussed earlier in this section, so that under deflection the blade is close to vertically aligned near rated speed for increased power capture. The blade would have curved upwind even more, but was prevented from curving beyond the blade root in lieu of a tip-strike reversal constraint. The maximum precurvature was also limited to 6.3 m for transportation reasons. Without that constraint, the same general shape and conclusion is drawn, but the curvature is more extreme leading to higher manufacturing and transportation costs. This type of upwind curvature is especially beneficial for upwind configurations because you get the same power benefit as you do in the downwind case, but you also increase the tower-strike margin whereas the downwind configuration moves the blade tips closer to the tower. In fact, several modern turbines use upwind curvature. Adding precurvature in the optimization decreased the cost of energy by an additional 2.5% beyond the corresponding design in Figure 4a.

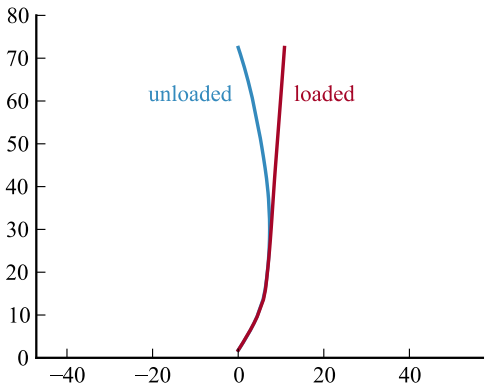

Figure 10. A downwind rotor blade with optimized precurvature shown both unloaded and loaded.

Wind Energ. 0000; **00**:1–16 © 0000 John Wiley & Sons, Ltd.
DOI: 10.1002/we
Prepared using weauth.cls

5. CONCLUSIONS

This research has focused on comparing upwind and downwind rotors for land-based turbines. Blade element momentum theory was used to model aerodynamics, and classical laminate theory with beam finite element analysis was used to model the structures. Nacelle, tower, and cost models were included to allow for assessment of cost of energy.

Traditional upwind designs become less efficient at larger rotor diameters and larger power ratings where the tower-strike constraint forces the blades to be very stiff. While upwind configurations still appear to be optimal for most of today's designs, as rotors become larger, machine ratings increase, and lower wind speed sites are more heavily utilized, downwind turbines provide some potential benefits. The results of the studies in this paper suggest that for Class III wind sites, significant savings in the structural mass of the blade are possible (around 25-30%). However, these benefits are somewhat offset by larger tower masses required for downwind configurations because the bending moment from the rotor-nacelle-assembly weight becomes additive to that of the bending moments from the rotor thrust. Additionally, the deflection of the blade under operational loading tends to decrease annual energy production. Still, modest savings in cost of energy of around 1-2% may be possible.

Large downwind precurvature was not seen to be beneficial within the parameters of this study. The large curvature did indeed decrease strain at operational conditions, but also decreased power production, margin against frequency constraints, and was less effective in reducing strain during survival load conditions. Optimally curved blades were actually curved upwind in order to maximize power capture. Downwind precurvature could be useful if the structural laminate was specifically optimized to provide stiff response near rated speed for high power capture, but responded flexibly at higher survival wind speeds.

Downwind rotors show potential for reduced cost of energy, but further research is needed to study the dynamic effects of the more flexible downwind blades. Only three-bladed concepts were explored in this study to allow more direct comparison to traditional upwind designs, but even greater mass reductions may be possible through downwind two-bladed designs. Further benefits would also result from airfoil shape optimization and composite laminate sequence tailoring. Additional studies are needed to quantify the impact of tower shadow on the designs, and explore concepts to alleviate the corresponding increase in fatigue. Improvements in the cost models and plant models are needed to capture other potential downwind turbine benefits such as simpler yaw systems and increased power capture in complex terrains. Penalties from the tower top bending moment could be reduced through more detailed drivetrain/nacelle design where the center of mass was shifted closer to the tower top. These and other improvements should be explored to better quantify the potential benefits and limitations of downwind turbines at utility-scale.

REFERENCES

1. Janajreh I, Qudaih R, Talab I, Ghenai C. Aerodynamic flow simulation of wind turbine: Downwind versus upwind configuration. *Energy Conversion and Management* Aug 2010; **51**(8):1656–1663, doi:10.1016/j.enconman.2009.12.013. URL http://dx.doi.org/10.1016/j.enconman.2009.12.013.
2. Reiso M, Muskulus M. The simultaneous effect of a fairing tower and increased blade flexibility on a downwind mounted rotor. *Journal of Renewable and Sustainable Energy* 2013; **5**(3):033 106, doi:10.1063/1.4803749. URL http://dx.doi.org/10.1063/1.4803749.
3. Yoshida S. Performance of downwind turbines in complex terrains. *Wind Engineering* Dec 2006; **30**(6):487–501, doi:10.1260/030952406779994169. URL http://dx.doi.org/10.1260/030952406779994169.
4. Reiso M, Moe G. Blade response on offshore bottom fixed wind turbines with down-wind rotors. *29th International Conference on Ocean, Offshore and Arctic Engineering: Volume 3*, ASME, 2010, doi:10.1115/omae2010-20586. URL http://dx.doi.org/10.1115/omae2010-20586.
5. Loth E, Steele A, Ichter B, Selig M, Moriarty P. Segmented ultralight pre-aligned rotor for extreme-scale wind turbines. *50th AIAA Aerospace Sciences Meeting including the New Horizons Forum and Aerospace Exposition*, 2012, doi:10.2514/6.2012-1290.
6. Wind turbines part 1: Design requirements. *Technical Report IEC 61400-1*, International Electrotechnical Commission 2005.
7. Ning A, Damiani R, Moriarty P. Objectives and constraints for wind turbine optimization. *Journal of Solar Energy Engineering* June 2014; **136**(4), doi:10.1115/1.4027693.
8. Ning A, Dykes K. Understanding the benefits and limitations of increasing maximum rotor tip speed for utility-scale wind turbines. *Journal of Physics: Conference Series* 2014; In press.
9. Guo Y, King R, Parsons T, Dykes K. A wind turbine drivetrain sizing and optimization model set. *Technical Report*, National Renewable Energy Laboratory, Golden, CO 2014. (forthcoming).

10. Dykes K. Development of wind turbine component mass-based cost models 2013. NREL Technical Report (not yet published).
11. Maples B, Hand M, Saur G. Land-based wind plant balance of station cost and scaling model 2013. NREL Technical Report (not yet published).
12. Fingersh LJ, Hand MM, Laxson AS. Wind turbine design cost and scaling model. *NREL/TP-500-40566*, National Renewable Energy Laboratory, Golden, CO December 2006.
13. Harrison R, Jenkins G. Cost modeling of horizontal axis wind turbines. *ETSU/W-34-00170-REP*, University of Sunderland December 1993.
14. Bywaters G, John V, Lynch J, Mattila P, Norton G, Stowell J, Salata M, Labath O, Chertok A, Hablanian D. Northern power systems WindPACT drive train alternative design study report. *NREL/SR-500-35524*, National Renewable Energy Laboratory October 2004.
15. Resor BR. Definition of a 5MW/61.5m wind turbine blade reference model. *SAND2013-2569*, Sandia National Laboratories April 2013.
16. Jonkman J, Butterfield S, Musial W, Scott G. Definition of a 5-MW reference wind turbine for offshore system development. *NREL/TP-500-38060*, National Renewable Energy Laboratory, Golden, CO Feb 2009.
17. Larwood SM. Dynamic analysis tool development for advanced geometry wind turbine blades. PhD Thesis, University of California Davis 2009.
18. Guideline for the certification of wind turbines. *Technical Report*, GL Renewables Certification 2010.
19. Halpin JC. *Primer on Composite Materials Analysis*. 2nd edn., Technomic, 1992.
20. Johnson A. *Handbook of Polymer Composites for Engineers*, chap. Structural Component Design Techniques. Woodhead Publishing, 1994.
21. Jonkman JM. Dynamics modeling and loads analysis of an offshore floating wind turbine. *Technical Report NREL/TP-500-41958*, National Renewable Energy Laboratory Dec 2007, doi:10.2172/921803. URL http://dx.doi.org/10.2172/921803.
22. European Committee for Standardisation. Eurocode 3: Design of steel structures—part 1-6: General rules—supplementary rules for the shell structures. *EN 1993-1-6: 20xx* 1993.
23. Guideline for the certification of offshore wind turbines. *Technical Report IV – Part 2, Chapter 6*, Germanischer Lloyd 2005.
24. Franco MD. Oems building bigger, better mousetraps. *North American Windpower* May 2014; **11**(5).
25. Gill PE, Murray W, Saunders MA. SNOPT: An SQP algorithm for large-scale constrained optimization. *SIAM review* 2005; **47**(1):99–131.
26. Gray J, Moore KT, Hearn TA, Naylor BA. Standard platform for benchmarking multidisciplinary design analysis and optimization architectures. *AIAA Journal* Feb 2013; **51**(10):2380–2394, doi:10.2514/1.J052160. URL http://dx.doi.org/10.2514/1.J052160.
27. Hascoët L, Pascual V. The Tapenade Automatic Differentiation tool: Principles, Model, and Specification. *ACM Transactions On Mathematical Software* 2013; **39**(3). URL http://dx.doi.org/10.1145/2450153.2450158.
28. Martins JRRA, Hwang JT. Review and unification of methods for computing derivatives of multidisciplinary computational models. *AIAA Journal* Oct 2013; **51**(11):2582–2599, doi:10.2514/1.J052184.
29. Gray J, Hearn T, Moore K, Hwang J, Martins J, Ning A. Automatic evaluation of multidisciplinary derivatives using a graph-based problem formulation in openmdao. *15th AIAA/ISSMO Multidisciplinary Analysis and Optimization Conference*, Atlanta, GA, 2014.